Electronic Supplementary Material (ESI) for Journal of Materials Chemistry C.

Promoting photoreduction selectivity via synergetic utilization between vacancy and nanofiber structure over flexible Zr/TiO_{2-x} nanofiber films

*Shan Jiang⁺, Haoze Li⁺, Wenke Gui, Yingbing Zhang, Chenchen Zhang, Lei Zhang, Jianping Yang and Li Wang**

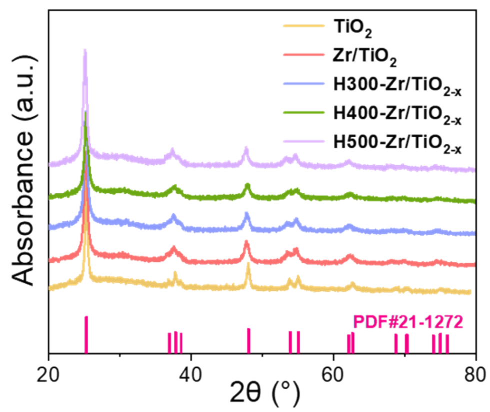

Figure S1. XRD patterns of the Zr/TiO_{2-x} NFs.

Element	Atomic Fraction (%)
Ti	35.66
O	54.69
Zr	9.65

Figure S2. TEM mapping of H400-Zr/TiO_{2-x} NFs.

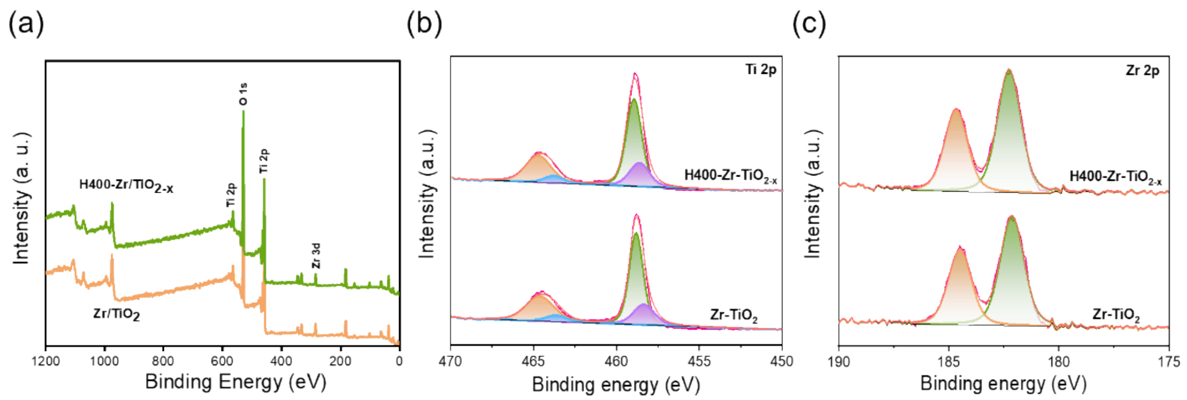

Figure S3. a) The full XPS spectra of Zr/TiO_2 NFs and H400-Zr/TiO_{2-x} NFs. b) Ti 2p and Zr 2p XPS spectra of Zr/TiO_2 NFs and H400-Zr/TiO_{2-x} NFs.

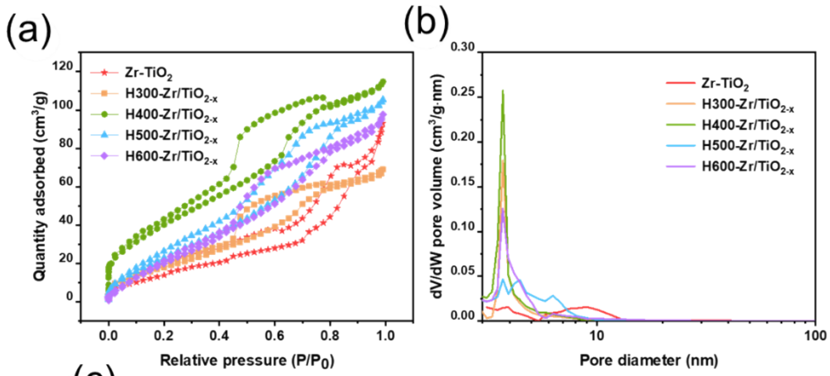

(c)

Sample	Surface area (m^2/g)	Pore size (nm)	Pore volume (cm^3/g)
Zr/TiO$_2$	67.3	8.5	0.14
H300-Zr/TiO$_{2-x}$	76.1	5.6	0.11
H400-Zr/TiO$_{2-x}$	158.6	4.5	0.18
H500-Zr/TiO$_{2-x}$	110.6	5.9	0.16
H600-Zr/TiO$_{2-x}$	107.8	5.6	0.15

Figure S4. a, b, c) N_2 adsorption-desorption isotherms that corresponded to SSA, pore diameters, surface area, pore size and pore volume of Zr-TiO$_{2-x}$ NFs.

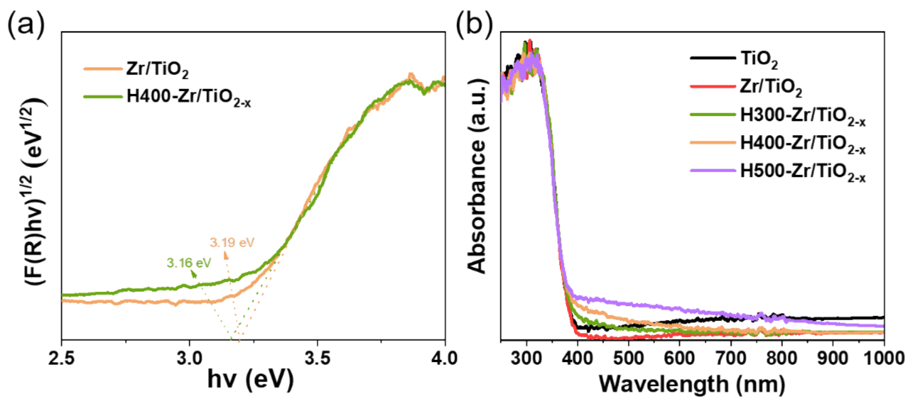

Figure S5. a) The band gap of Zr/TiO$_2$ NFs and H400-Zr/TiO$_{2-x}$ NFs. b) UV-visible diffuse reflectance spectra of Zr/TiO$_{2-x}$ NFs.

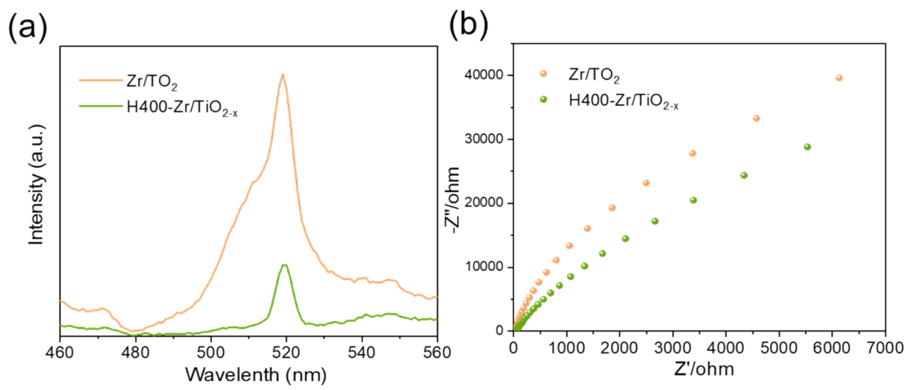

Figure S6. a) PL spectra and b) EIS spectra of Zr/TiO$_2$ NFs and H400-Zr/TiO$_{2-x}$ NFs.

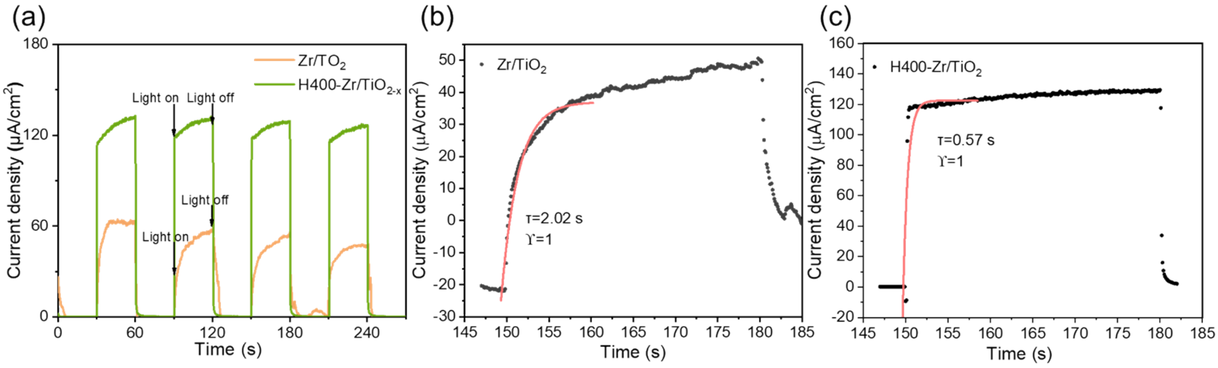

Figure S7. a) photocurrent curves of Zr/TiO$_2$ NFs and H400-Zr/TiO$_{2-x}$ NFs. b) Acquiring the rise time of Zr/TiO$_2$ NFs by fitting the on curve. c) Acquiring the rise time of H400-Zr/TiO$_{2-x}$ NFs by fitting the on curve.

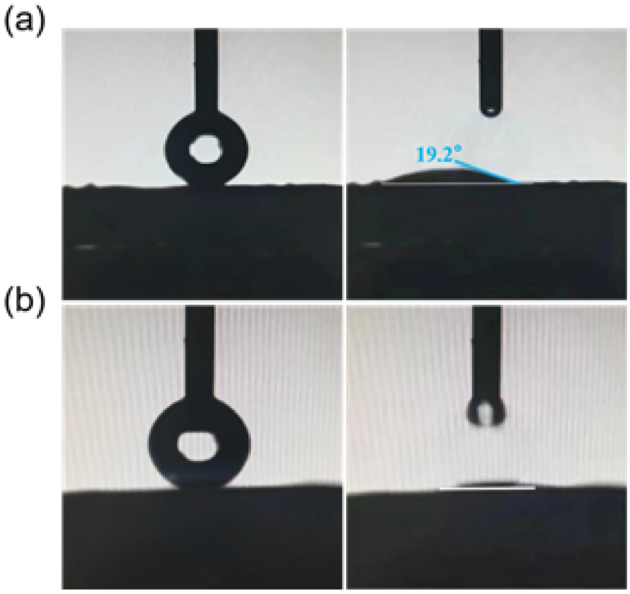

Figure S8. a, b) Comparison of the water wettability of Zr/TiO$_2$ and H400-Zr/TiO$_{2-x}$ NFs.

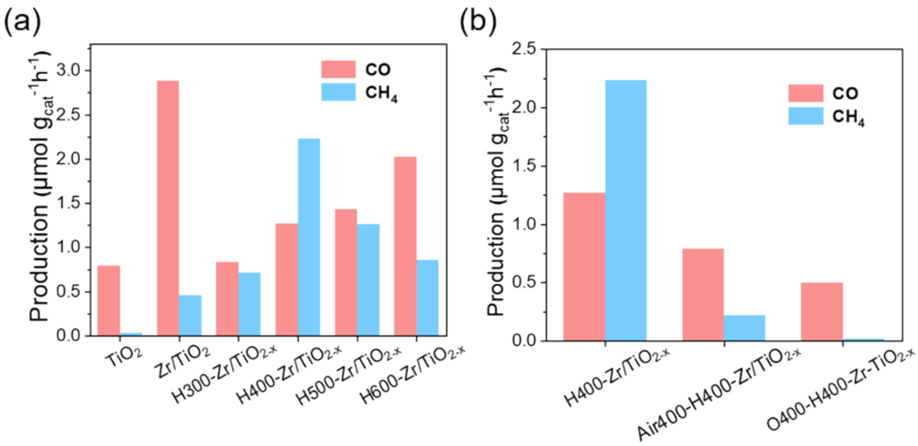

Figure S9. a) Yield rate of photocatalytic CO_2 reduction over various Zr/TiO$_{2-x}$ NFs materials. d) Yield rate of H400-Zr/TiO$_{2-x}$ and H400-Zr/TiO$_{2-x}$ post-treated with different content of O_2 to remove OVs.

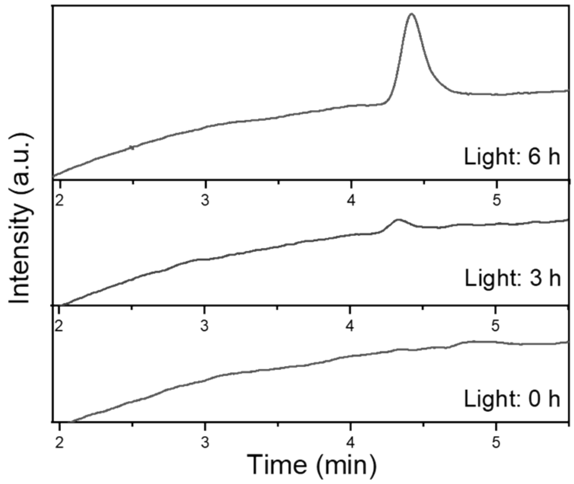

Figure S10. Peak change of O_2 in gas chromatography during photocatalysis of H400-Zr/TiO_{2-x} NFs.

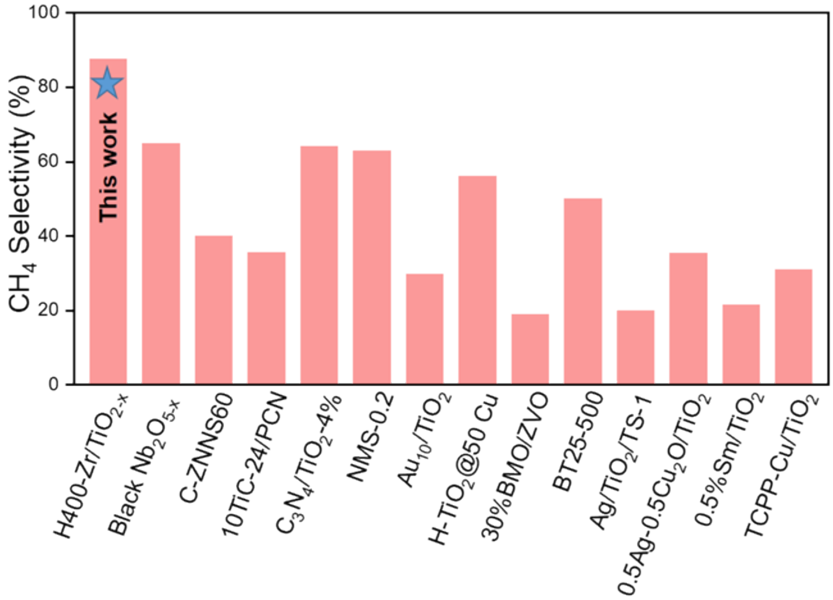

Figure S11. Comparison of photocatalytic CH_4 selectivity with other catalysts towards CO_2 reduction reported in the literature. [1-13]

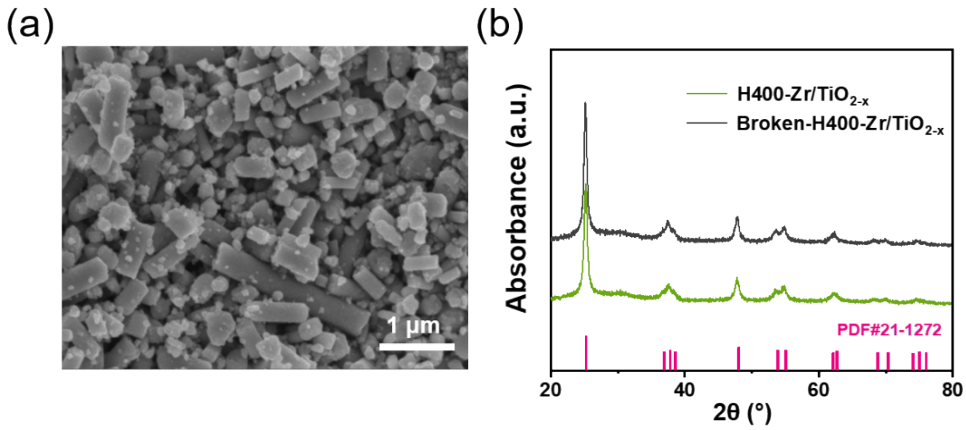

Figure S12. a) SEM images of crushed H400-Zr/TiO_{2-x} NFs. b) XRD patterns of crushed H400-Zr/TiO_{2-x} NFs.

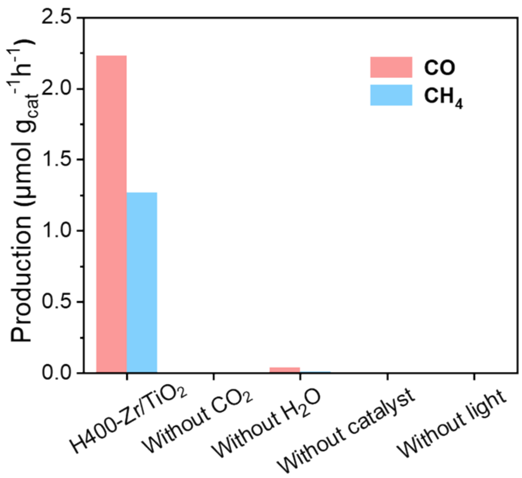

Figure S13. The gas evolution under different situations of H400-Zr/TiO_{2-x} NFs.

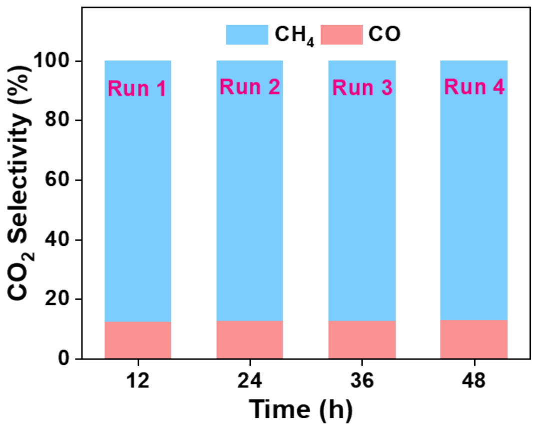

Figure S14. Cycling selective stability of CO_2 over H400-Zr/TiO_{2-x} NFs.

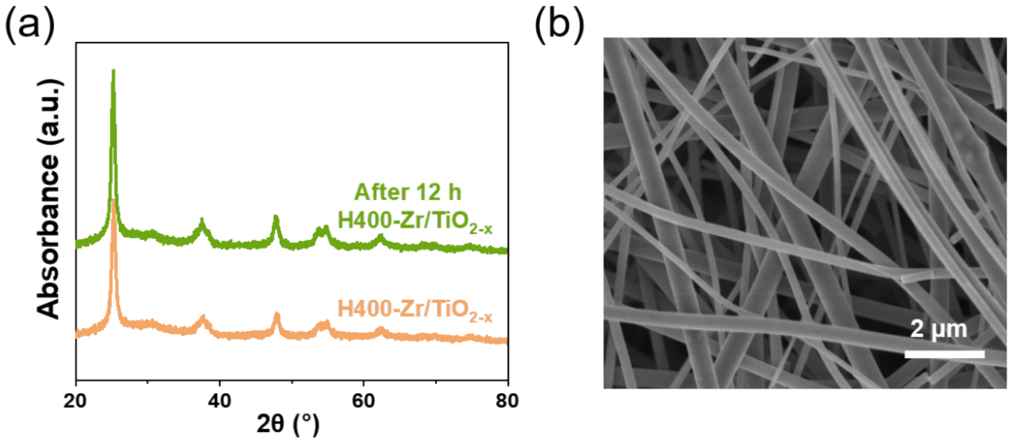

Figure S15. a) XRD patterns of H400-Zr/TiO_{2-x} NFs before and after photocatalytic reduction process. b) SEM image of H400-Zr/TiO_{2-x} NFs after photocatalytic reduction process.

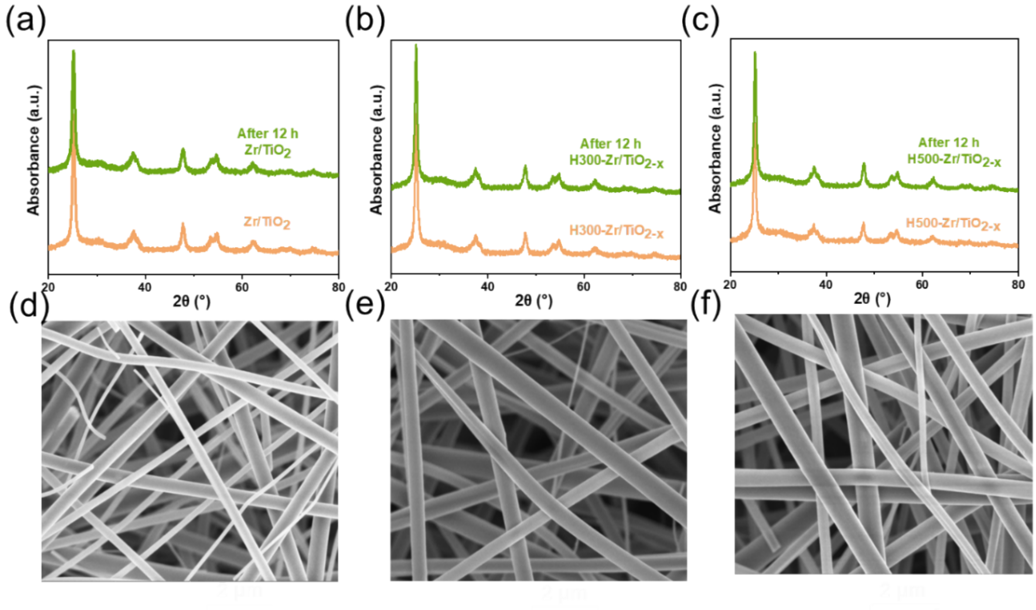

Figure S16. Comparison before and after reaction XRD patterns and SEM images of Zr/TiO_{2-x} NFs.

Figure S17. a, b) Folding and opening processes of H400-Zr/TiO_{2-x} NFs. c) The comparison on the yield rates of CO and CH_4 over H400-Zr/TiO_{2-x} NFs before and after floding.

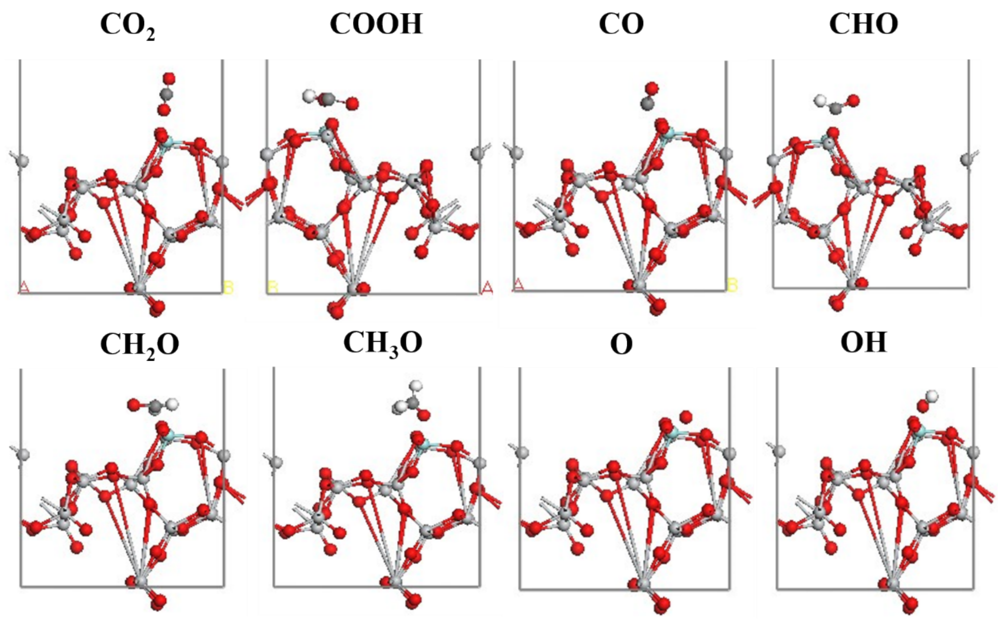

Figure S18. Structural models of Gibbs free energy calculations for the H400-Zr/TiO_{2-x} NFs.

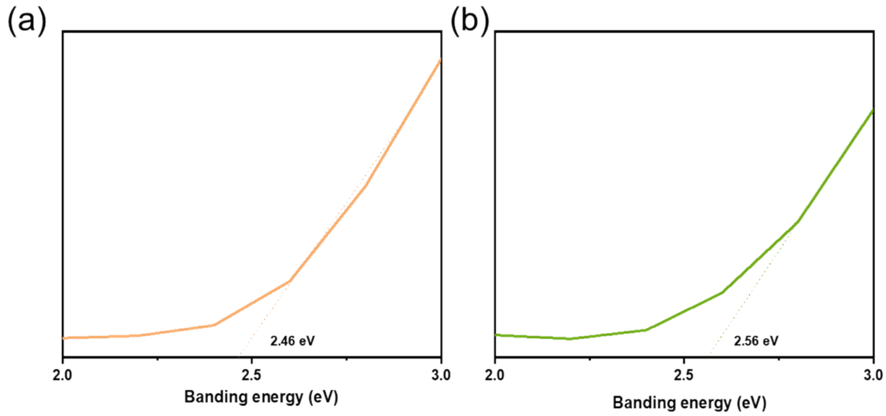

Figure S19. XPS VB spectra of Zr/TiO_2 and H400-Zr/TiO_{2-x} NFs.

Table S1. Free energy (eV) and total energy (eV) of CO_2 photoreduction for the H400-Zr/TiO_{2-x} NFs.

	$*CO_2$	COOH*	CO*	CHO*	CH_2O*	CH_3O*	*OH	H_2O*
E-TS /eV	-1036.60	-1050.16	-595.88	-610.26	-628.15	-642.10	-430.63	-471.64

H400-Zr/TiO_{2-x}	CO_2	$*CO_2$	COOH*	CO*	CO	CHO*	CH_2O*	CH_3O*	O*	*OH	H_2O*
E-TS /eV	-38886.10	-39923.01	-39929.84	-39482.02	-38885.12	-39496.68	-39508.91	-39528.81	-38886.46	-39318.29	-39358.56
G/eV	0	-0.3091	6.4202	-0.0445	0.9657	-0.3208	5.3346	-0.6181	-0.3599	-1.5621	-0.8270

References

[1] Y. Li, A. G. Walsh, D. Li, D. Do, H. Ma, C. Wang, P. Zhang, X. Zhang, *Nanoscale* 2020, **12**, 17245-17252.

[2] H. Peng, R. Guo, H. Lin, *J. Rare Earth* 2020, **38**, 1297-1304.

[3] C. Huang, R. Guo, W. Pan, J. Tang, W. Zhou, H. Qin, X. Liu, P. Jia, *J. CO_2 Util*. 2018, **26**, 487-495.

[4] M. Liu, L. Zheng, X. Bao, Z. Wang, P. Wang, Y. Liu, H. Cheng, Y. Dai, B. Huang, Z. Zheng, *Chem. Engin. J.* 2021, **405**, 126654.

[5] L. Chen, K. Huang, Q. Xie, S. M. Lam, J. C. Sin, T. Su, H. Ji, Z. Qin, *Catal. Sci. Technol*. 2021, **11**, 1602-1614.

[6] F. Xu, J. Zhang, B. Zhu, J. Yu, J. Xu, *Appl. Catal. B: Environ.* 2018, **230**, 194-202.

[7] G. Ren, Z. Wei, Z. Li, X. Zhang, X. Meng, *Mater. Today Chem.* 2023, **27**,101260.

[8] H. Zhao, X. Zheng, X. Feng, *Y. Li, J. Phys. Chem. C* 2018, **122**, 18949-18956.

[9] H. Feng, C. Zhang, M. Luo, Y. Hu, Z. Dong, S. Xue, P. K. Chu, *Nanoscale* 2022, **14**, 16303-16313.

[10] Z. Jiang, W. Sun, W. Miao, Z. Yuan, G. Yang, F. Kong, T. Yan, J. Chen, B. Huang, C. An, G. A. Ozin, *Adv. Sci.* 2019, **6**, 1900289.

[11] R. Sun, X. Jiang, M. Zhang, Y. Ma, X. Jiang, Z. Liu, Y. Wang, J. Yang, M. Xie, W. Han, *J. Catal.* 2019, **378**, 192-200.

[12] Z. Zhang, J. Tan, L. Cheng,W. Yang, *Ceram. Int.* 2021, **47**, 34106-34114.

[13] X. Lin, S. Xia, L. Zhang, Y. Zhang, S. Sun, Y. Chen, S. Chen, B. Ding, J. Yu, J. Yan, *Adv. Mater.* 2022, **34**, 2200756.